Pharmaceutical Research, Vol. 24, No. 9, September 2007 (© 2007)
DOI: 10.1007/s11095-007-9276-6

Research Paper

Focused-ion-beam Milling: A Novel Approach to Probing the Interior of Particles Used for Inhalation Aerosols

Desmond Heng,[1,3] Patricia Tang,[1] Julie M. Cairney,[2] Hak-Kim Chan,[1,4] David J. Cutler,[1] Rania Salama,[1] and Jimmy Yun[3]

Received October 5, 2006; accepted February 16, 2007; published online April 3, 2007

Purpose. The current study aimed to examine the pharmaceutical applications of the focused-ion-beam (FIB) in the inhalation aerosol field, particularly to particle porosity determination (i.e. percentage of particles having a porous interior).
Materials and Methods. The interior of various spray dried particles (bovine serum albumin (BSA) with different degrees of surface corrugation, mannitol, disodium cromoglycate and sodium chloride) was investigated via FIB milling at customized conditions, followed by viewing under a high resolution field-emission scanning electron microscope. Two sets of ten particles for each sample were examined.
Results. For the spray-dried BSA particles, a decrease in particle porosity (from 50 to 0%) was observed with increasing particle surface corrugation. Spray-dried mannitol, disodium cromoglycate and sodium chloride particles were determined to be 90–100%, 0–10% and 0% porous, respectively. The porosity in the BSA and mannitol particles thus should be considered for the aerodynamic behaviour of these particles.
Conclusions. The FIB technology represents a novel approach useful for probing the interior of particles linking to the aerosol properties of the powder. Suitable milling protocols have been developed which can be adapted to study other similar particles.

KEY WORDS: dry powder aerosol; focused-ion-beam miller; porous particles; spray drying; surface corrugation.

INTRODUCTION

The focused-ion-beam (FIB) technique has been used in the semi-conductor industry for over a decade (1,2), where its use includes circuit design, circuit diagnostics and failure analysis (1,3–5). In the more general materials science domain, its applications are just as widespread, encompassing micro-structural analysis (2,6–9), transmission electron microscopy specimen preparation (10–13), thickness determination of coatings (11) and micromachining (2).

A FIB is architecturally similar to a scanning electron microscope; however, instead of an electron source, it utilizes a liquid metal ion source (i.e. typically gallium) as the filament to produce a finely-focused (5 nm) beam of energetic metal ions that can be operated either at low beam currents for high resolution imaging or precise milling, or higher beam currents for coarser and faster milling (13,14). Liquid metal ion sources are favored over gas discharge sources because they give much higher brightness, and are able to produce ion beams with high current densities and small beam diameters (6). The present study was performed using a dual-beam FIB-SEM (scanning electron microscope) instrument. This instrument interfaces an ion column and an electron column at a 52° angle to each other on a single microscope platform. Interaction of either the electron beam or the ion beam with the specimen produces secondary electrons which are detected and used to form an image (13). Images generated with the ion beam display different contrast mechanisms, depth of focus and sensitivity to surface topography (1,5,6) compared to images generated by the electron beam. Therefore both ion-generated and electron-generated images are useful in providing complementary information (5,6). However, the ion beam, even when used at low beam currents, will always remove material from the specimen surface. This deleterious effect is not severe in very hard, robust materials, but can sometimes preclude the use of the ion beam for imaging in softer materials. The dual-beam instrument offers a distinct advantage in that use of the electron beam allows the specimens to be imaged without the damaging effects of the ion beam. This is particularly important when delicate specimens, such as the pharmaceutical particles investigated in the present study, are being examined. Another advantage of the dual beam system over a single ion beam system is that, due to the difference in

[1] Faculty of Pharmacy, A15, The University of Sydney, NSW 2006, Sydney, Australia.
[2] The Australian Key Centre for Microscopy and Microanalysis, The University of Sydney, NSW 2006, Sydney, Australia.
[3] Nanomaterials Technology Pte. Ltd., 28 Ayer Rajah Crescent, #03-03, Singapore, 139959, Singapore.
[4] To whom correspondence should be addressed. (e-mail: kimc@pharm.usyd.edu.au)

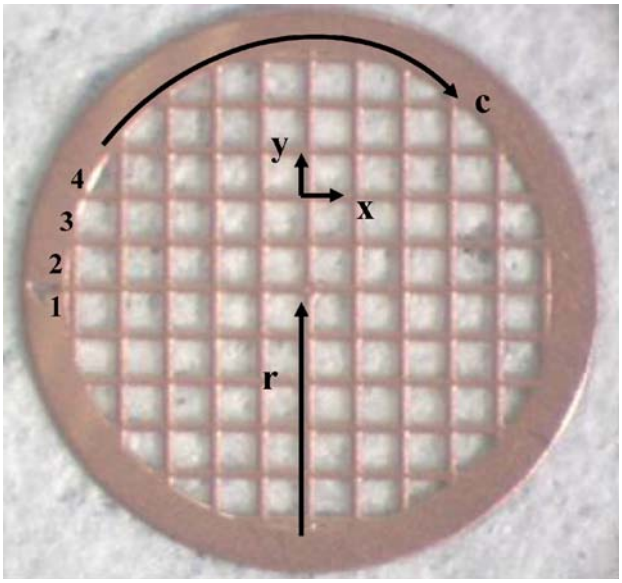

Fig. 1. Illustration of the random sampling of particles via a four coordinate system. *c*, *r*, *x* and *y* denotes the circumferential, radial, *x* and *y* coordinates, respectively.

orientation of the two columns, cross-sections prepared with the ion beam may be immediately imaged using the electron beam without any movement of the specimen.

The strengths of the FIB lie in its high positional accuracy of milling (i.e. less than 0.1 μm) at the specific point of interest (3), ability to prepare a uniform cross-section in heterogeneous samples (1), and the added capability of surface imaging with the ion or electron beam (3). Even though dual beam instruments are highly suited for the milling of fragile or porous specimens, their use in this regard has not been fully exploited. Application of this technique to the biological and soft material domain is still evolving (1). The limited investigations in this area include studies of the internal morphology of human hair (3), small arthropods (3,6), bone cells on a biomaterial (1), microspheres (4), and animal tissues and cells (15,16). More recently, the technology has even been proposed as a useful alternative to cryo-ultramicrotomy of frozen hydrated biological samples (17).

Over the last decade, there has been an increasing trend towards the use of 'porous' particles to enhance the aerosol performance of powders (18–21). These particles have a small aerodynamic diameter due to their inherent low particle density, and are quite often 'rough' on their surfaces (19,20,22). Previously, our group (22) had shown that a slight degree of surface corrugation enhanced the aerosol performance of a powder. Evidence based on freeze fracture and confocal microscopy led to the conclusion that the particles were solid (23,24). These classical methods (1,23,24) used for study of the particle interior tend to introduce artifacts (1) and have tedious and long development times (e.g. successful incorporation of the fluorescence dye into the material for fluorescence confocal microscopy). The advent of the FIB technique has since provided us with the opportunity to further probe the interior of these particles. To the authors' knowledge, FIB had been applied to powders (10,25,26) and porous catalytic membranes (27), but never directly to the inhalation aerosol field.

In this paper, we investigated the use of the FIB technology to analyze the particle interior of the following inhalation aerosol powders: bovine serum albumin (different degree of surface corrugation), mannitol, disodium cromoglycate and sodium chloride. Bovine serum albumin is commonly used as a model protein in aerosol research (24), mannitol for bronchial provocation testing in asthmatics and for the enhancement of mucociliary clearance in both normal and asthmatic subjects (23), disodium cromoglycate in the prophylaxis of asthma (28) and lastly, sodium chloride as an osmotic agent in bronchial provocation tests for asthmatics (29).

MATERIALS AND METHODS

Preparation of Powders

All powders were prepared via spray drying (Buchi 191, Flawil, Switzerland) at atomization and aspiration rates of 800 l/h and 57.6 m^3/h, respectively, unless otherwise stated.

Bovine Serum Albumin (BSA)

Bovine serum albumin (Fraction V, minimum 98%, Sigma Chemical Co., St. Louis, MO, USA) was dissolved in deionized water (MilliQ, Waters) and the solution was spray dried at an inlet temperature of 45°C (outlet temperature 36°C) and feed rate of 1.4 ml/min. As previously described (22), the feed concentration and atomization rate were

Table I. FIB Milling Parameters for the Powders

	Powder							
	BSA		Mannitol		DSCG		NaCl	
	Mill	Clean	Mill	Clean	Mill	Clean	Mill	Clean
Accelerating Voltage (kV)	20	5	10	5	20	5	20	5
Beam Current (pA)	210	14	16	14	210	14	23	2
Mill Depth (nm) (Based on Silicon)	500	10	70	10	500	10	500	10

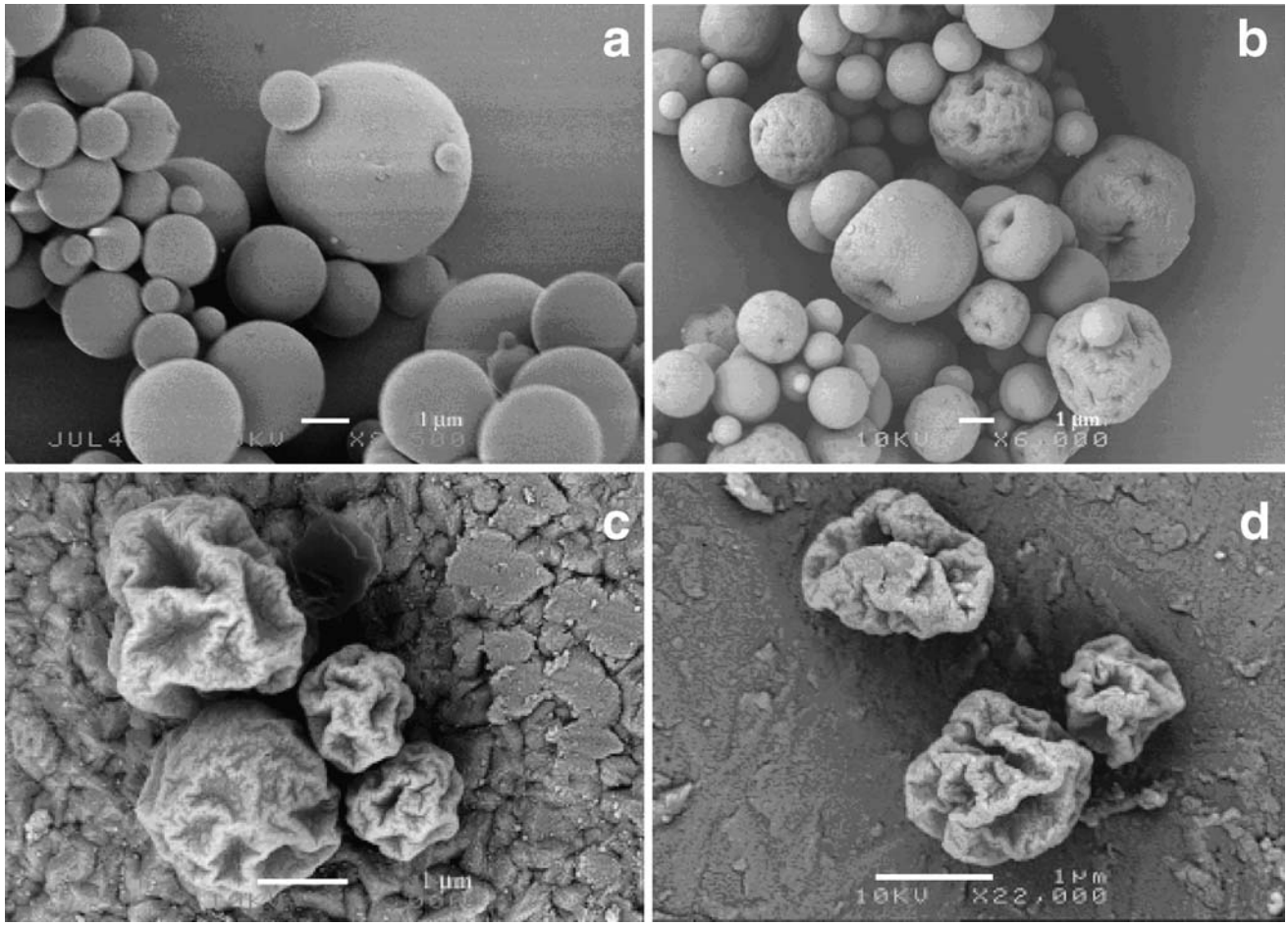

Fig. 2. Secondary electron images of unsectioned spray dried bovine serum albumin particles having increasing degree of surface corrugation, as shown from photos (**a**–**d**), respectively.

adjusted to yield particles with increasing degrees of surface corrugation. The different degrees of surface corrugation was previously quantified via fractal analysis (22).

Mannitol

Mannitol (USP Grade, Roquette, France) was dissolved in deionized water (MilliQ, Waters) and the solution (10 mg/ml) was spray dried at an inlet temperature of 110°C (outlet temperature 75–78°C) and a feed rate of 1.4 ml/min (23).

Disodium Cromoglycate

Disodium cromoglycate (DSCG) (Sanofi-Aventis, England) was dissolved in deionized water (MilliQ, Waters) and the

Table II. Different Degrees of Porosity for Spray-dried Bovine Serum Albumin (Degree of Surface Corrugation Increases from *i* to *iv*), Mannitol, Disodium Cromoglycate and Sodium Chloride Particles

Random Sample Set (of 10 Particles)	Number of Particles with Porous Interior (Distinct Hole or Concaved)						
	BSA				Mannitol	DSCG	NaCl
	i	*ii*	*iii*	*iv*			
1	5	4	1	0	9	1	0
2[a]	5	4	2	0	10	0	0
% Porosity	50	40	10–20	0	90–100	0–10	0

[a] repeated set

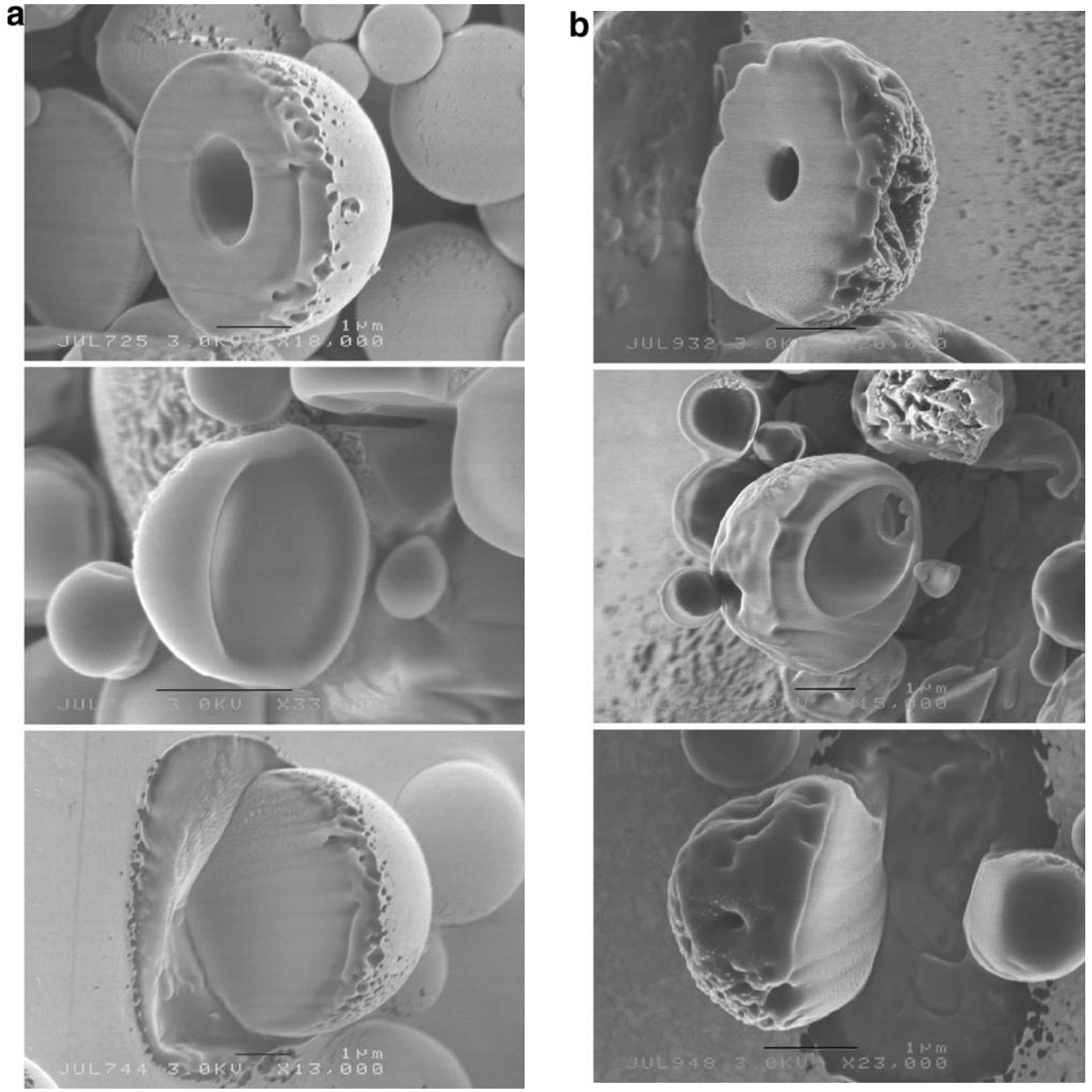

Fig. 3. Secondary electron images of the FIB cross-sections of spray dried bovine serum albumin particles with increasing degree of surface corrugation (**a**–**d**) after FIB milling; scale bar 1 μm.

solution (10 mg/ml) was spray dried at an inlet temperature of 140°C (outlet temperature 70–75°C), feed rate of 4 ml/min and atomization rate of 700 l/h.

Sodium Chloride

As described previously (29), an ultrasonicated NaCl suspension (AR Grade NaCl powder, 99% purity, LabServ, Australia) was spray dried at an inlet temperature of 90°C (outlet temperature 55–62°C), feed rate of 4.40 ± 0.47 ml/min and atomization rate of 550 l/h. During spray drying, the suspension was continuously stirred at 1,000 rpm.

Random Sampling

Random sampling of the particles was carried out as follows: Particle positioning was determined via the use of a 100-mesh transmission electron microscopy (TEM) grid (GCu100, ProSciTech, Australia) as the reference background and a 4-coordinate system: circumferential (28 segments), radial (5 segments), x (10 segments) and y (10 segments) (Fig. 1). A random list of the 4-coordinate system was generated by a four-dimension random number generator (Minitab Inc., release 13, for Windows). Two sets of ten particles were randomly sampled for each species and

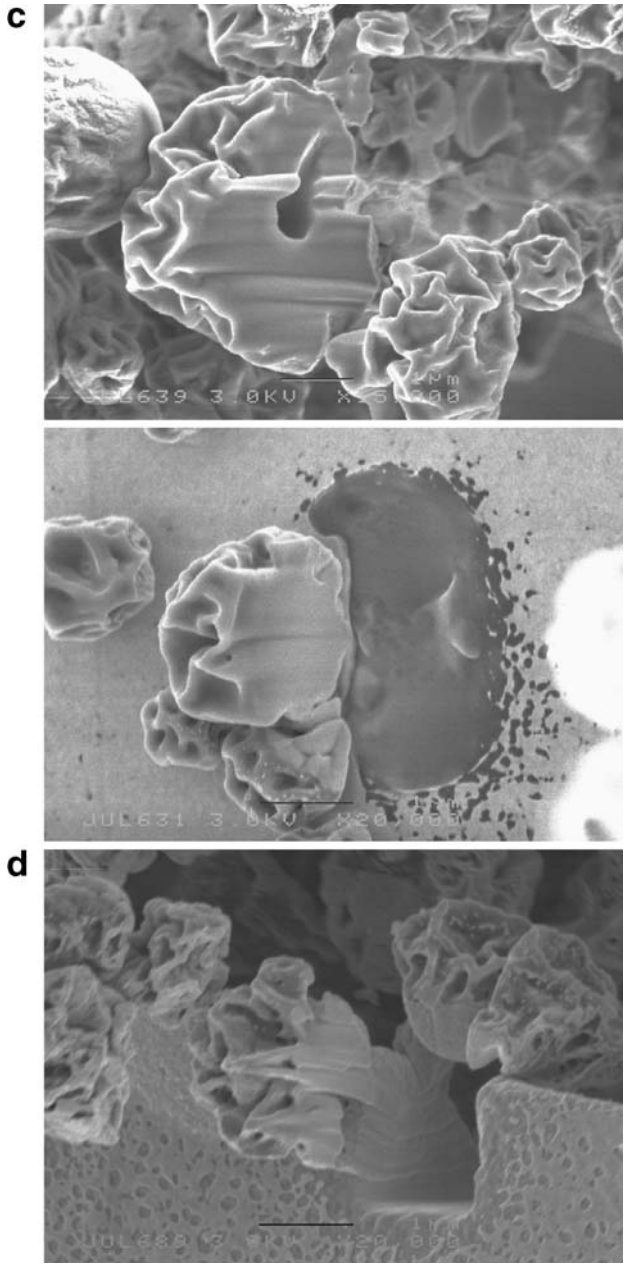

Fig. 3. (Continued).

compared. Particles were considered to be porous if they had a distinct hole or a concaved interior. Porosity was expressed as the number of particles having a porous interior regardless of the size of the hole or cavity.

Focused-ion-beam Milling and Scanning Electron Microscope Imaging

FIB milling of the samples was performed in a focused-ion-beam/scanning electron microscope dual beam system (Quanta 200 3D, FEI, USA). As each material had different degrees of softness and fragility, milling conditions was adjusted for each material. The specific milling parameters altered were; accelerating voltage, beam current and mill depth (Z) (Table I). The powder samples were mounted onto a 100-mesh transmission electron microscopy (TEM) grid (GCu100, ProSciTech, Australia) (Fig. 1). The samples were coated with platinum/gold (50 nm thick), mounted onto the stage with a thin layer of double-sided adhesive carbon tape. Milling (vertical cutting) of the samples was carried out at a stage tilt of 52°.

The samples were examined under a high resolution field emission scanning electron microscope (Jeol JSM 6000F, Japan) at 3–10 kV. The samples were tilted from 0 to −30° or +30° for visualization of the right or left cut surface, respectively.

Technical Considerations

The milling process was carried out via a 2-step approach: initial milling and final cleaning (14,30). Both milling stages consisted of stepwise material removal line by line, where the last area to be milled is in the direct vicinity to the cross-sectional face being prepared. The final cleaning stage was performed at the lowest possible combination of beam current, accelerating voltage and mill depth to minimize surface artifacts (30).

Accelerating Voltages. While this FIB system usually operates at 30 kV, an accelerating voltage of 20 kV was used in the initial milling stage because it was less damaging to the soft specimens (i.e. the interaction volume of the Ga^+ ions is smaller at lower accelerating voltages (31)). An even lower accelerating voltage of 10 kV was used for mannitol because the material was extremely soft and therefore highly susceptible to irradiation damage. Lower accelerating voltages (<10 kV) were not useful for the milling stage as very little material was removed (4). The cleaning stage utilized an accelerating voltage of 5 kV, which was in line with the manufacturer's recommendations (14).

Beam Currents. The high beam currents used in the milling of metal- and silicon-based specimens were not applicable to the present soft specimens, as their weak beam-blanking tails would inevitably cause sputtering damage outside the desired milling area (3). The lowest possible beam currents (e.g. 2 pA–0.21 nA) were used as they caused much less beam irradiation damage to the areas outside of the regions specified for milling due to both a finer probe size and minimal damage from the beam-blanking tails (3), were observed to be less prone to charging up, and drifted little on the specimens (3). However, as milling times were inversely proportional to the beam current strength, a compromise had to be made to the optimal beam current which would allow for a practical exposure time under the ion beam (i.e. the lowest beam currents required impractically long exposure periods). Milling times for the present samples were typically kept under 5 min. An extremely low beam current (i.e. 14 pA) was used in the final cleaning stage to suit the demands of the precise polishing/cleaning step (14). The beam currents used for the milling of mannitol and NaCl particles were reduced (i.e. 16 pA and 23 pA, respectively) because mannitol particles were rather soft and highly susceptible to

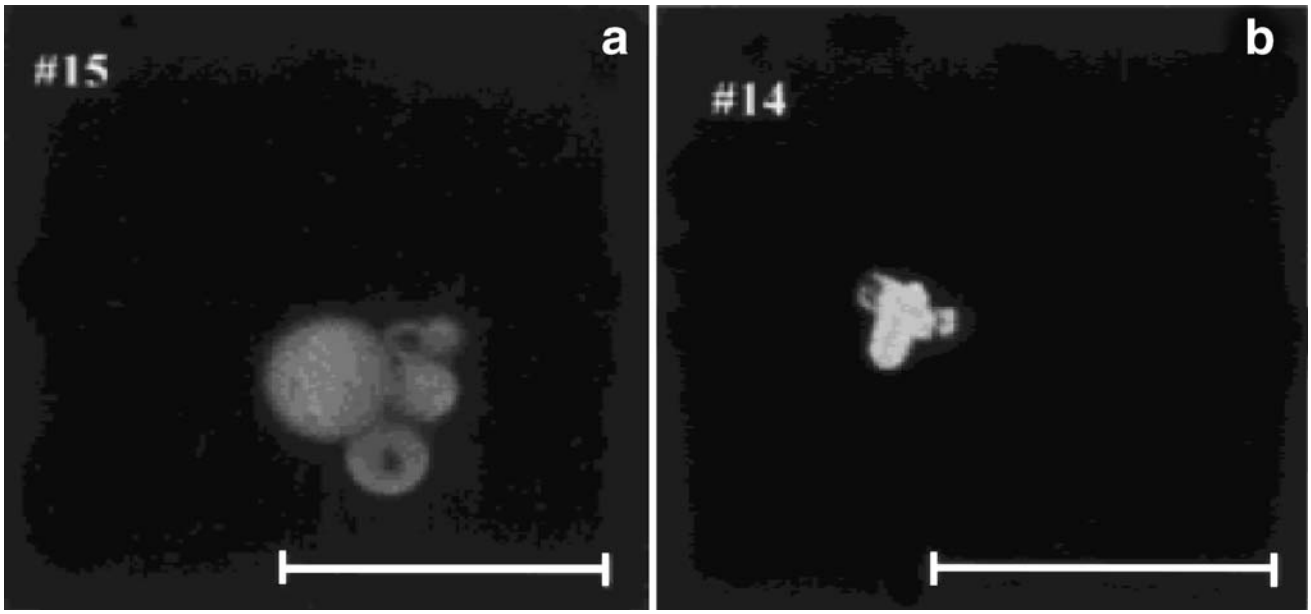

Fig. 4. Confocal images of (**a**) spherical and (**b**) corrugated bovine serum albumin particles; scale bar 10 μm. (adapted from Chew *et al*., 2001, (24), with the permission of Springer Science and Business Media).

the formation of milling artifacts such as "waterfalling" (13), and the NaCl particles were smaller (i.e. 1–2 μm), requiring lower milling times.

Mill Depths. Larger mill depths (longer milling periods for a given beam current and accelerating voltage) have been shown to result in higher levels of damage in fragile specimens (3). The present author also observed, empirically, a greater degree of waterfalling artifacts in specimens which were milled for longer periods (larger mill depths). For this reason, the minimum mill depth required to cut through the entire particle was used in each case. The mill depth (based on silicon) for mannitol was lower than that required for the other materials because this material was much softer than the rest of the materials and mills very quickly. A lower mill depth was therefore sufficient in making the cut while ensuring minimal exposure time under the ion beam.

RESULTS AND DISCUSSION

BSA Particles

For the BSA particles (Fig. 2), the degree of interior porosity was found to decrease with increasing surface corrugation (Table II). Fig. 3 shows the interior features of these particles: distinct hole, concaved or solid, with holes being more frequently observed than concaved ones. The smooth to slightly corrugated particles reveal all these features (Fig. 3a and b, respectively), whereas the interior of the moderately corrugated particles (Fig. 3c) show only hole or solid, and the highly corrugated particles are totally solid (Fig. 3d). The close agreement between the sampled sets (i.e. difference of less than two particles) reflected the robustness of the sampling method. The porosity (i.e. distinct hole or concaved) rate was 50% for the smooth particles, 40% for the slightly corrugated particles, 10–20% for the moderately corrugated particles, and none for the highly corrugated ones (Table II). These findings, which are contrary to the previous evidence based on confocal microscopy suggesting only solid interior (i.e. due to the ambiguity of the confocal images) (24) (Fig. 4), indicate that depending on the corrugation, BSA particles can actually be partly hollow and the degree of porosity should hence be taken into consideration for their aerodynamic behaviour. A slight increase in surface corrugation was previously shown to enhance the fine particle fraction (FPF) significantly from 27 to 41%, and further increase in corrugation showed not much improvement in the FPF (22). The present findings suggest that the lack of further improvement may be due to these corrugated particles being solid (instead of hollow), otherwise they would have a smaller aerodynamic diameter and hence higher FPF.

The images in Fig. 3 display some 'waterfalling' artifacts (characteristic of ion-sputtered materials) on the cut surface of the moderately and highly corrugated BSA particles (Fig. 3c and d), despite the same milling condition being used throughout for all the BSA particles. This 'waterfalling' effect or topographical irregularity (31) was due to the channeling of the ion beam in samples which were not homogeneous (i.e. uneven surface) or had internal/external impurities (e.g. dust/dirt, small inclusions or precipitates), and often began in the form of planes, steps, spikes or cone-like structures (32,33). An uneven or rough surface would cause certain areas to mill faster than others, hence, contributing to the 'waterfalling' effect. This topographical irregularity was observed only on the surfaces of the more corrugated particles whereas the smooth particles were relatively free from it.

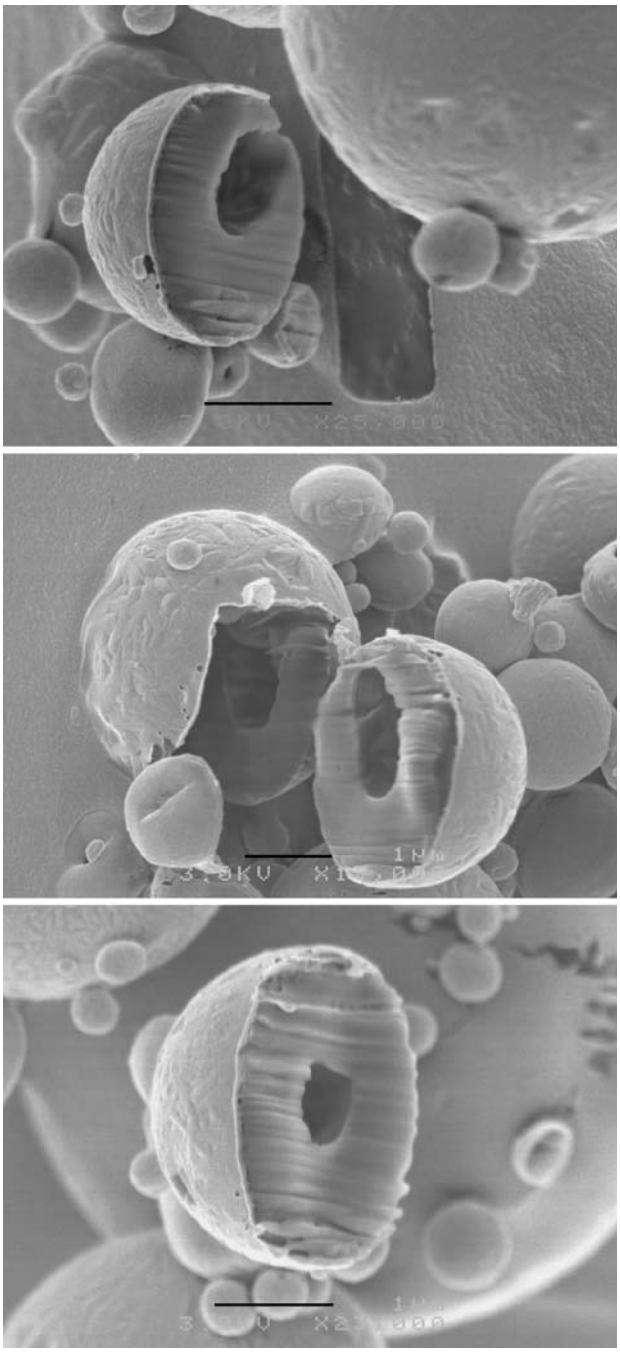

Fig. 5. Secondary electron images of the FIB cross-sections of spray dried mannitol particles after FIB milling; scale bar 1 μm.

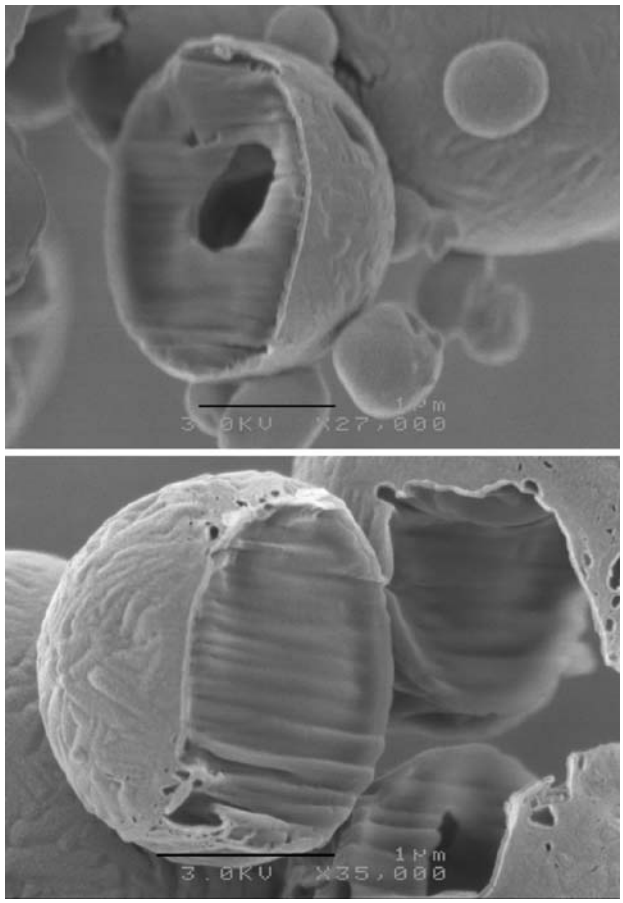

Fig. 5. (Continued).

Mannitol Particles

FIB revealed that 90–100% of these particles are porous (Table II and Fig. 5), an observation contrary to previous results based on freeze fracture (23) (Fig. 6) which suggested that these particles were completely solid. Although not produced using the same equipment and experimental conditions, spray dried mannitol particles have more recently been shown as porous (34,35) by confocal laser scanning microscopy and density measurements (35). The present results thus highlighted the applicability of the FIB as a complementary tool in porosity determination.

The image in Fig. 5 also displays 'waterfalling' artifacts on the cut surface of the mannitol particles. Generally, the

Fig. 6. Transmission electron image of a freeze fractured mannitol particle. (Adapted from Chew *et al*., 1999, (23), with the permission of Springer Science and Business Media).

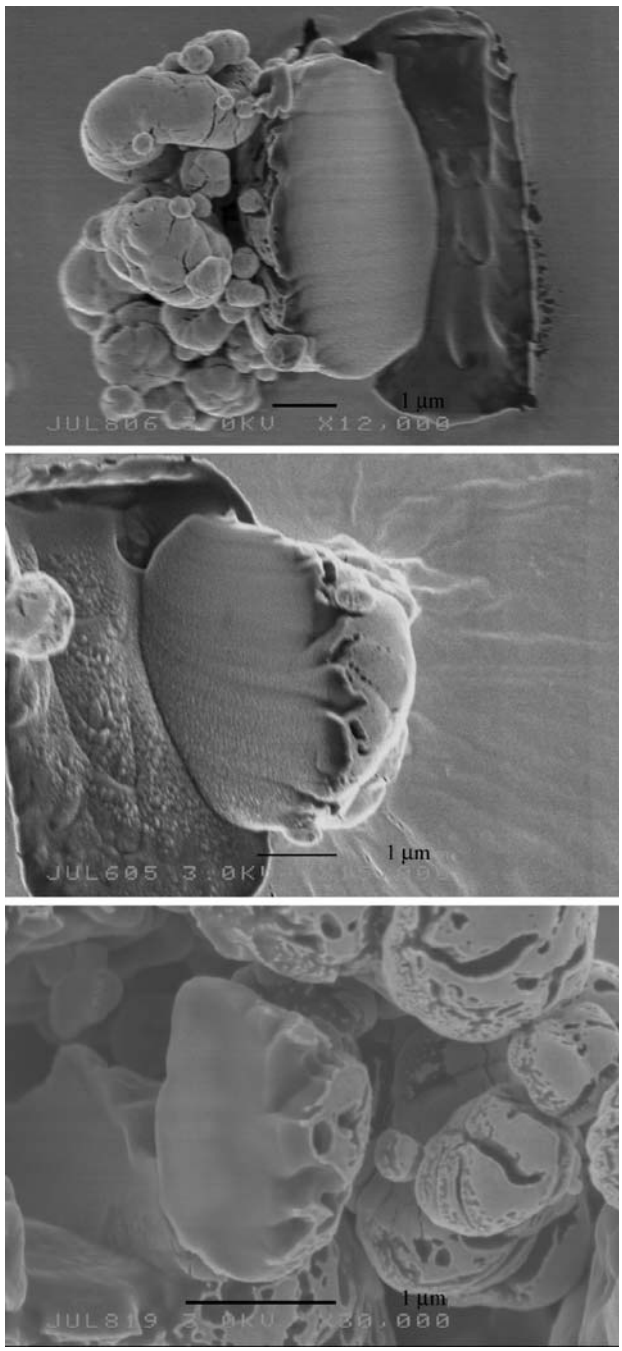

Fig. 7. Secondary electron images of the FIB cross-sections of spray dried disodium cromoglycate particles after FIB milling.

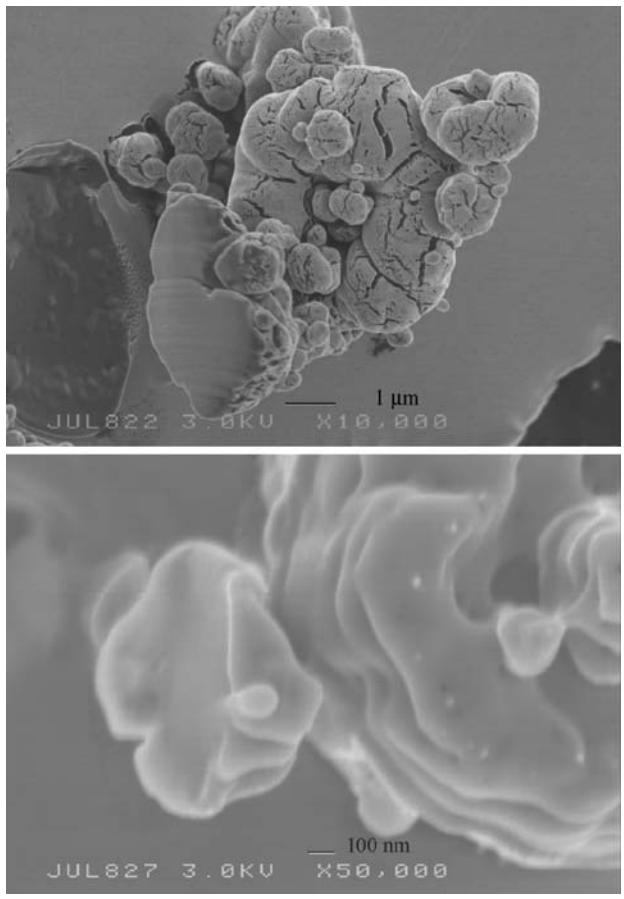

Fig. 7. (Continued).

softer the material, the greater the degree of channeling of the energetic gallium ion beam, and the increased frequency of artifact formation (8). Hence, this high degree of channeling suggested that mannitol was a very soft material. Even though the final 'cleaning' mill at a lower beam current (Table I) was aimed at minimizing these 'waterfalling' effects (30), it is apparent that the additional step was inadequate in instances where the particles were very soft (or highly corrugated as in BSA).

DSCG and NaCl Particles

FIB milling revealed that spray dried DSCG particles had a porosity rate of 0–10% (Table II and Fig. 7). The NaCl particles were completely solid (Table II and Fig. 8), which was expected as they were single crystals. The cut surfaces of the DSCG and NaCl particles were less prone to FIB-induced artifacts, exhibiting no topographical irregularities, as they were neither as soft as mannitol nor were they corrugated. Since these particles were relatively non-porous in contrast to BSA and mannitol, it indicates that porosity is influenced by the production process used and/or the material's inherent properties.

CONCLUSIONS

The FIB cutting of particles used in inhalation aerosols results in a distinct and uniform cross-section, which provide complementary information to (and may even offer distinct advantages over) those derived via classical preparation methods like freeze fracture and confocal microscopy (23,24). The present study showed that BSA and mannitol particles were partly hollow and hence should be taken into consideration for their aerodynamic behaviour. The ability to dissect and probe the interior of particles will aid inhalation aerosol scientists in obtaining a more complete picture of the particle. It is

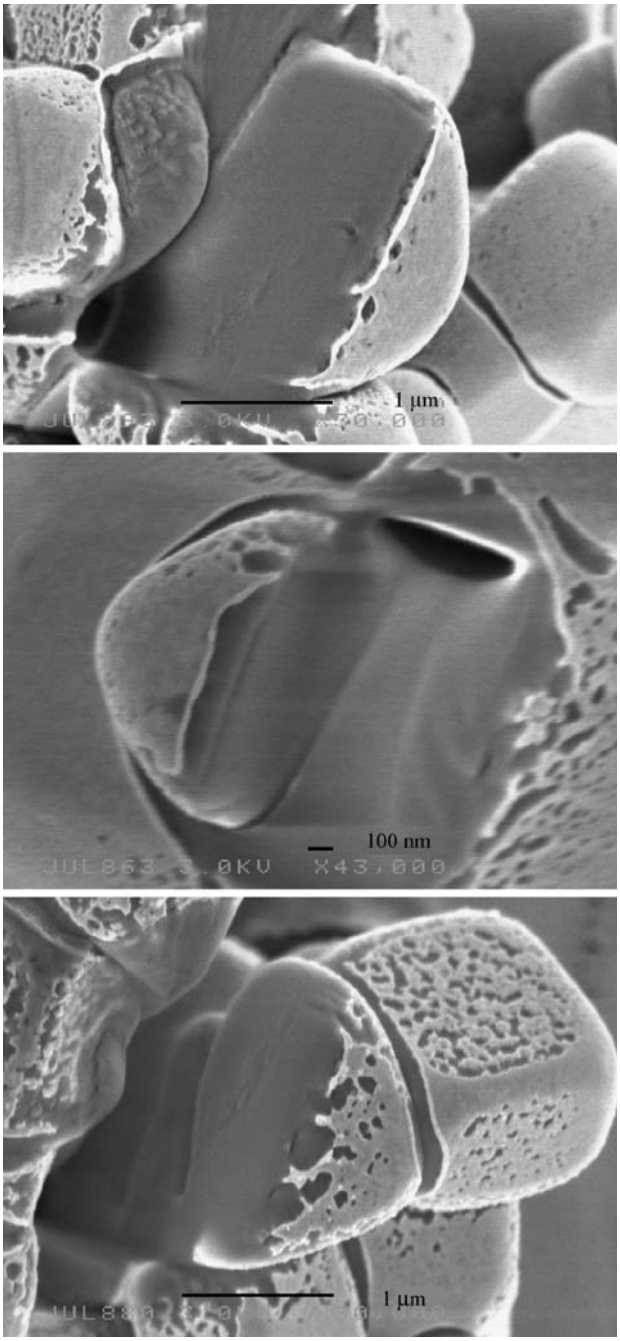

Fig. 8. Secondary electron images of the FIB cross-sections of spray dried sodium chloride particles after FIB milling.

envisaged that the FIB method developed here for inhalation aerosol particles can be readily applied to other types of 'soft' non-inhalation drug particles.

ACKNOWLEDGEMENTS

The authors are grateful to Errin Johnson, Toshi Arakawa, Adam Sikorski, Ian Kaplin, Tony Romeo, Emine Korkmaz and Robert Mair of the Electron Microscope Unit (The University of Sydney) for their valuable advice and assistance in the area of microscopy. This work was supported by a grant from the Australian Research Council (ARC Linkage Project LP 0561675 with Nanomaterials Technology Pte. Ltd). DH was a recipient of the Australian Postgraduate Award (Industry).

REFERENCES

1. D. J. Stokes, F. Morrissey, and B. H. Lich. A new approach to studying biological and soft materials using focused ion beam scanning electron microscopy (FIB SEM). *J. Phys.* **26**:50–53 (2006).
2. P. R. Munroe and J. M. Cairney. The application of focused ion beam milling for electron microscope preparation. *Proceedings of Materials 98: The Biennial Conference of the Institute of Materials Engineering, Australasia*, 1998, pp. 457–462.
3. T. Ishitani, H. Hirose, and H. Tsuboi. Focused-ion-beam digging of biological specimens. *J. Electron Microsc.* **44**:110–114 (1995).
4. S. H. Moghadam, R. Dinarvand, and L. H. Cartilier. The focused ion beam technique: a useful tool for pharmaceutical characterization. *Int. J. Pharm.* **321**:50–55 (2006).
5. J. Melngailis. Critical review: Focused ion beam technology and applications. *J. Vac. Sci. Technol., B***5**:469–495 (1987).
6. R. J. Young, T. Dingle, K. Robinson, and P. J. A. Pugh. An application of scanned focused ion beam milling to studies on the internal morphology of small arthropods. *J. Microsc.* **172**:81–88 (1993).
7. L. Holzer, F. Indutnyi, P. H. Gasser, B. Munch, and M. Wegmann. Three-dimensional analysis of porous BaTiO3 ceramics using FIB nanotomography. *J. Microsc.* **216**:84–95 (2004).
8. P. R. Munroe, J. M. Cairney, and R. D. Smith. Application of the focused ion beam miller to the characterization of composite materials, *Composites in the Transportation Industry ACUN-2, International Composites Conference, Sydney, Australia*, 2000, pp. 486–494.
9. J. M. Cairney, P. R. Munroe, and D. J. Sordelet. Microstructural analysis of a FeAl/quasicrystal-based composite prepared using a focused ion beam miller. *J. Microsc.* **201**:201–211 (2001).
10. J. M. Cairney and P. R. Munroe. Preparation of transmission electron microscope specimens from FeAl and WC powders using focused-ion beam milling. *Mater. Charact.* **45**:1–8 (2001).
11. J. M. Cairney and P. R. Munroe. Redeposition effects in TEM sample preparation of FeAl-based metal matrix composites using the focused ion beam miller. *Microsc. Microanal.* **6**:514–515 (2000).
12. A. Barna, B. Pecz, and M. Menyhard. TEM sample preparation by ion milling/amorphization. *Micron* **30**:267–276 (1999).
13. J. M. Cairney, R. D. Smith, and P. R. Munroe. Transmission electron microscope specimen preparation of metal matrix composites using the focused ion beam miller. *Microsc. Microanal.* **6**:452–462 (2000).
14. M. Dufek. The Quanta 200 3D user's operation manual, 3rd edition, 2004, pp. 5–4, 5–42.
15. D. Drobne, M. Milani, M. Ballerini, A. Zrimec, M. Berden Zrimec, F. Tatti, and K. Draslar. Focused ion beam for microscopy and *in situ* sample preparation: application on a crustacean digestive system. *J. Biomed. Opt.* **9**:1238–1243 (2004).
16. D. Drobne, M. Milani, A. Zrimec, V. Leser, and M. Berden Zrimec. Electron and ion imaging of gland cells using the FIB/SEM system. *J. Microsc.* **219**:29–35 (2005).
17. M. Marko, C. Hsieh, W. Moberlychan, C. A. Mannella, and J. Frank. Focused ion beam milling of vitreous water: prospects for an alternative to cry-ultramicrotomy of frozen-hydrated biological samples. *J. Microsc.* **222**:42–47 (2006).
18. T. E. Tarara, J. G. Weers, and L. A. Dellamary. Engineered powders for inhalation. In R. N. Dalby, P. R. Byron, S. J. Farr, and J. Peart (eds.), *Respiratory Drug Delivery VII, Vol. 2*, Serentec, Raleigh, North Carolina, 2000, pp. 413–415.
19. R. Vanbever, J. D. Mintzes, J. Wang, J. Nice, D. Chen, R. Batycky, R. Langer, and D. A. Edwards. Formulation and physical characterisation of large porous particles for inhalation. *Pharm. Res.* **16**:1735–1742 (1999).
20. Y. F. Maa, P. A. Nguyen, T. Sweeney, S. J. Shire, and C. C. Hsu. Protein inhalation powders: spray drying vs spray freeze drying. *Pharm. Res.* **16**:249–254 (1999).

21. L. A. Dellamary, T. E. Tarara, D. J. Smith, C. H. Woelk, A. Adractas, M. L. Costello, H. Gill, and J. G. Weers. Hollow porous particles in metered dose inhalers. *Pharm. Res.* **17**:168–174 (2000).
22. N. Y. K. Chew, P. Tang, H. K. Chan, and J. A. Raper. How much particle surface corrugation is sufficient to improve aerosol performance of powders? *Pharm. Res.* **22**:148–152 (2005).
23. N. Y. K. Chew and H. K. Chan. Influence of particle size, airflow, and inhaler device on the dispersion of mannitol powders as aerosols. *Pharm. Res.* **16**:1098–1103 (1999).
24. N. Y. K. Chew and H. K. Chan. Use of solid corrugated particles to enhance powder aerosol performance. *Pharm. Res.* **18**:1570–1577 (2001).
25. B. I. Prenitzer, L. A. Giannuzzi, K. Newman, S. R. Brown, R. B. Irwin, T. L. Shofner, and F. A. Stevie. Transmission electron microscope specimen preparation of Zn powders using the focused ion beam lift-out technique. *Metall. Mater. Trans., A* **29A**:2399–2406 (1998).
26. J. K. Lomness, L. A. Giannuzzi, and M. D. Hampton. Site-specific transmission electron microscope characterization of micrometer-sized particles using the focused ion beam lift-out technique. *Microsc. Microanal.* **7**:418–423 (2001).
27. A. J. Smith, P. R. Munroe, T. Tran, and M. S. Wainwright. FIB preparation of a sensitive porous catalyst for TEM elemental mapping at high magnifications. *J. Mater. Sci.* **36**:3519–3524 (2001).
28. H. K. Chan and I. Gonda. Aerodynamic properties of elongated particles of cromoglycic acid. *J. Aerosol Sci.* **20**:157–168 (1988).
29. P. Tang, H. K. Chan, E. Tam, N. de Gruyter, and J. Chan. Preparation of NaCl powder suitable for inhalation. *Ind. Eng. Chem. Res.* **45**:4188–4192 (2006).
30. J. M. Cairney, P. R. Munroe, and J. H. Schneibel. Examination of fracture surfaces using focused ion beam milling. *Scr. Mater.* **42**:473–478 (2000).
31. D. J. Barber. Radiation damage in ion-milled specimens: characteristics, effects and methods of damage limitation. *Ultramicroscopy* **52**:101–125 (1993).
32. R. S. Nelson and D. J. Mazey. Surface damage and topography changes produced during sputtering. In R. Behrisch, W. Heiland, W. Poschenrieder, P. Staib, and H. Verbeek (eds.), *Ion Surface Interaction, Sputtering and Related Phenomena*, Gordon and Breach, UK, 1973, pp. 199–206.
33. L. Brown. Radiation damage in ion-milled specimens: characteristics, effects and methods of damage limitation. *Radiat. Effects* **98**:101–125 (1986).
34. A. Grenha, B. Seijo, and C. Remunan-Lopez. Microencapsulated chitosan nanoparticles for lung protein delivery. *Eur. J. Pharm. Sci.* **25**:427–437 (2005).
35. J. Elversson and A. Millqvist-fureby. Particle size and density in spray drying—effects of carbohydrate properties. *J. Pharm. Sci.* **94**: 2049–2060 (2005).